No. 936

Map Projection Errors in the Weber Problem

by

Yoshiaki Ohsawa and Takeshi Koshizuka

June 2001

Map Projection Errors in the Weber Problem

Yoshiaki OHSAWA
Takeshi KOSHIZUKA

Institute of Policy and Planning Sciences
University of Tsukuba
Tsukuba 305-8573, JAPAN
phone: +81-298-53-5224
fax: +81-298-55-3849
e-mail: osawa@sk.tsukuba.ac.jp.

June 29, 2001

Abstract

True demand data lie on the surface of the earth. However, most of their location are given not by spherical but planar data which are obtained from a map projection. Some distortions occur as a result of using these planar location data. The objective of this paper is to analyze how cylindrical projections cause the distortion in the Weber problem where all the demand points are distributed on the Northern Hemisphere. First, we demonstrate that planar solutions are always located on the south of the spherical solution if we choose Mercator projection, or equirectangular or equal-area projections with standard parallels near the demand data. Second, we verify that this geographical tendency is inclined to hold as the demand points are distributed symmetrical or widely or toward the north, although we choose other standard parallels.

Key words
Weber problem; spherical distance; cylindrical projections; map projection error

1. INTRODUCTION

As economical, political, industrial and transportation systems become progressively more global, locational analysis on the surface of a sphere becomes more important. In answer to this issue, Drezner and Wesolowsky (1978), Litwhiler and Aly(1979,1980), Love et al.(1988), Xue(1994), Hansen et al.(1995) have formulated spherical Weber problems. In their formulations, demand points and the facility to be located are on the surface of a sphere, and that transportation costs are measured based on great circle distances.

Although true demand data are distributed on the surface of the earth, most of their locations are expressed by planar coordinates produced by some type of map projection. In the extreme case, such planar data are only available for actual facility planning. Since there are no map that can accurately represent the distances between all pair of points on a sphere, the spherical Weber problem is essentially different from any planar Weber problem. As a result, an error is incurred if planar demand data are used, as pointed out in Litwhiler and Aly(1979). Accordingly, the validity of the conclusions drawn employing the planar data are questionable. Thus, the examination of such an error is important in locational analysis. In this paper, the error is called a *map projection error*. Litwhiler and Aly (1979) showed that using planar data generated by an equirectangular projection instead of spherical data results in serious projection errors based on some small-size computational experiments. In contrast to their numerical work, the goal of this paper is to characterize the projection errors theoretically. Surprisingly, there has previously been no formal analysis to clarify the characteristics of such projection error theoretically, as far as we are aware.

We concentrate on the case where all the demand points are located on the Northern Hemisphere. This is because many countries are situated in either the Northern or Southern Hemisphere only. We also specifically deal with three cylindrical projections, namely, *Mercator*, *equirectangular* and *cylindrical equal-area* projections. Examples of these projections are presented in Figures 1, 2 and 3, respectively. The Tissot's indicatrices, which measure how angular and area distortions occur in the map projections, are also displayed. These projections and the indicatrices are explained in McDonell(1991), Snyder(1993), Bugayevskiy and Snyder(1995). There are two reasons for concentrating on these map projections. First, they are so well-known that they can be found in most standard textbooks of cartography, and their transformation formulae are very simple to construct and interpret. Hence, a number of different cylindrical projections are proposed based on them. Their use from a historical point

of view is stated in detail in Snyder(1993). Second, they have different special properties such as *conformality*, *equidistance* and *equal-area*, which affect map selection for certain purposes. The principal advantage of Mercator projection is conformality, so it has been applied to navigator charts for 400 years. As shown in Figure 1, all Tissot's indicatrices are given by circles, indicating that there is no local angular distortion at every points. Equirectangular projection, which is sometimes called the *cylindrical equidistant projection*, has the benefit of scale precision on all the meridians and on the two parallels. It has been used in general atlases and small area maps such as city and country maps. Since equal-area projection preserves area size, it has been used to show statistical density data. As presented in Figure 3, all Tissot's indicatrices are shown by circles or ellipses of the same area, leading to no area distortion at every points.

This paper is organized as follows. Section 2 describes the formulations and the solution methods for spherical and planar Weber problems. Also, the computational examples for three moderately large regions on the Northern Hemisphere, namely, the European Union, the United States and Japan are discussed and interpreted. Section 3 provides the theoretical results for explaining the computational results. Section 4 contains our conclusions. All the proofs are collected in the Mathematical Appendix for convenience.

In this paper we set up a system of traditional latitude-longitude coordinate in order to specify the locations of points on the surface of a sphere, and a system of Cartesian coordinate to express the ones in a plane. For clarity, we represent the Cartesian coordinate as $(\cdot, \cdot)$ and the latitude-longitude one as $\{\cdot, \cdot\}$.

2. WEBER PROBLEMS AND PROJECTION ERRORS

2.1. Spherical Weber problem

Let $\mathbf{p}_1 = \{\phi_1, \lambda_1\}, \cdots, \mathbf{p}_n = \{\phi_n, \lambda_n\}$ be the distinct demand points on the surface of the Northern Hemisphere whose radius is normalized to equal one. We define the demand set S by $S \equiv \{\mathbf{p}_1, \mathbf{p}_2, \cdots, \mathbf{p}_n\}$, and the index set I by $I \equiv \{1, \ldots, n\}$. Let ω_i be the weight of i-th demand point. Then the *spherical Weber problem* is formulated as follows:

$$\min_{\mathbf{p}} SW(\mathbf{p}) \equiv \sum_{i \in I} \omega_i \delta(\mathbf{p}_i, \mathbf{p}), \tag{1}$$

where $\mathbf{p} \equiv \{\phi, \lambda\}$ is the location of the facility on the surface of a sphere to be set up, and $\delta(\mathbf{p}, \mathbf{p}_i)$ is the great circle distance between $\mathbf{p}$ and $\mathbf{p}_i$.

We may assume that local spherical solution for the set S is located on the prime meridian without loss of generality. So we denote it by $\mathbf{p}^* \equiv \{\phi^*, 0\}$. There are now two cases on the location of $\mathbf{p}^*$, *floating case*: $\mathbf{p}^* \notin S$; and *absorbed case*: $\mathbf{p}^* \in S$: see Boltyanski et al.(1999). In the floating case, the spherical solution does not coincide with any demand point and in general it cannot be expressed analytically.

Throughout the rest of the paper, we take the following assumptions: (a1) they are covered by a spherical disk with a radius of $\pi/4$; and (a2) the demand set can not create the absorbed cases. The spherical Weber problem may have local as well as global minimizers due to the nature of the non-convexity of the objective function $SW(\mathbf{p})$ in (1). Drezner and Wesolowsky (1978) showed that if all the demand points are covered by a spherical disk with a radius of $\pi/4$, then a local minimizer is also global. Therefore, assumptions (a1) and (a2) mean that we can concentrate on the global solution in floating case. Similar results for local minimum and/or for the absorbed cases can be obtained but the presentation is rather complicated.

2.2. Planar Weber problem

Let $\mathrm{f}(\mathbf{p}) \equiv (f_x(\mathbf{p}), f_y(\mathbf{p}))$ be the planar image of $\mathbf{p}$ on the surface of a sphere under a map projection f. The *planar Weber problem* generated by the map projection can be expressed as follows:

$$\min_{\mathbf{p}} PW(\mathbf{p} : S) \equiv \sum_{i \in I} \omega_i d(\mathrm{f}(\mathbf{p}_i), \mathrm{f}(\mathbf{p})), \tag{2}$$

where $d(\mathrm{f}(\mathbf{p}_i), \mathrm{f}(\mathbf{p}))$ is the Euclidean distance between the planar images $\mathrm{f}(\mathbf{p}_i)$ and $\mathrm{f}(\mathbf{p})$. Note that its optimal location cannot be always expressed analytically, as in the spherical Weber problem.

As shown in Love et al.(1988) and Boltyanski et al.(1999), the partial derivative of $PW(\mathbf{p})$ evaluated at the spherical solution is expressed by

$$\frac{\partial PW(\mathbf{p} : S)}{\partial y}\Big|_{\mathbf{p}=\mathbf{p}^*} \equiv -\sum_{i \in I} \omega_i \frac{f_y(\mathbf{p}_i) - f_y(\mathbf{p}^*)}{d(\mathrm{f}(\mathbf{p}_i), \mathrm{f}(\mathbf{p}^*))}. \tag{3}$$

Since $\frac{\mathrm{f}(\mathbf{p}_i) - \mathrm{f}(\mathbf{p}^*)}{d(\mathrm{f}(\mathbf{p}_i), \mathrm{f}(\mathbf{p}^*))}$ is the rooted unit vector from $\mathrm{f}(\mathbf{p}^*)$ in the direction of $\mathrm{f}(\mathbf{p}_i)$, the derivative can be expressed as the weighted sum of the y-th coordinate of such vectors, i.e, y-th direction force component. This partial derivative gives the slope of the tangent to the objective function $PW(\mathbf{p})$ at the spherical solution $\mathbf{p}^*$ along the prime meridian toward the North pole. Hence, $\frac{\partial PW(\mathbf{p}:S)}{\partial y}\Big|_{\mathbf{p}=\mathbf{p}^*} > 0$ means that the south becomes the direction of decrease in

the planar objective function at the spherical solution, i.e., the spherical solution is worse than some points of its southern neighborhood in terms of that planar Weber problem. Thus, in order to show that most planar solutions are located on the south of the spherical one, we shall prove $\frac{\partial PW(\mathbf{p}:S)}{\partial y}|_{\mathbf{p}=\mathbf{p}^*} > 0$.

On orthographic projections the surface of a sphere is projected with parallel rays on a perpendicular plane, so it has been employed for maps of celestial bodies: see McDonell(1991), Snyder(1993), Bugayevskiy and Snyder(1995). An example of this projection is given in Figure 4. Its advantage is that all great circle arcs passing through the center are shown as straight lines. Its another advantage is that the bearing from the center to all the points on the surface are preserved. Based on these advantages, Litwhiler and Aly(1980) demonstrated that the planar solution on the orthographic projection centered on the spherical solution becomes the spherical solution. Under the orthographic projection centered on $\mathbf{p}^* = \{\phi^*, 0\}$, $\mathbf{p} \equiv \{\phi, \lambda\}$ on a sphere is transformed into

$$\mathbf{g}(\mathbf{p}) \equiv (g_x(\mathbf{p}), g_y(\mathbf{p})) \equiv (\cos\phi \sin\lambda, \sin\phi^* \cos\phi[1 - \cos\lambda] + \sin(\phi - \phi^*)). \tag{4}$$

The result by Litwhiler and Aly(1980) together with inequality (3) leads to $\sum_{i\in I} \omega_i \frac{g_y(\mathbf{p}_i) - g_y(\mathbf{p}^*)}{d(\mathbf{g}(\mathbf{p}_i), \mathbf{g}(\mathbf{p}^*))} = 0$ in floating cases. Therefore, $\frac{\partial PW(\mathbf{p}:S)}{\partial y}|_{\mathbf{p}=\mathbf{p}^*} > 0$ if

$$\frac{f_y(\mathbf{p}_i) - f_y(\mathbf{p}^*)}{d(\mathbf{f}(\mathbf{p}_i), \mathbf{f}(\mathbf{p}^*))} < \frac{g_y(\mathbf{p}_i) - g_y(\mathbf{p}^*)}{d(\mathbf{g}(\mathbf{p}_i), \mathbf{g}(\mathbf{p}^*))}, \qquad \forall i \in I, \tag{5}$$

which will be useful in our succeeding analysis.

We examine map projection errors generated by Mercator, equirectangular and equal-area projections. As shown in Bugayevskiy and Snyder(1995), Mercator projection transforms $\mathbf{p} \equiv \{\phi, \lambda\}$ on the spherical surface into $(\lambda, \ln[\tan(\pi/4 + \phi/2)])$. The last two projections produce a variety of maps by varying the location of standard parallels. *Standard lines* are defined as lines which do not change length when projected from a generating sphere to a map. The image of $\mathbf{p}$ under the equirectangular projections is $(\lambda \cos\theta, \phi)$, where θth parallel $(0 \leq \theta < \pi/2)$ is standard. Its image under the equal-area projection with standard parallel at θ is $(\lambda \cos\theta, \sin\phi/\cos\theta)$. Note that Behrmann projection and Peters projection are special cases of the cylindrical equal-area projection, as pointed out in Snyder(1993). In Figures 2 and 3, the standard parallels are placed at 30° and the center lines are fixed at 135°E.

As shown in Figures 1, 2 and 3, these three projections are composed of an evenly spaced network of horizontal parallels and vertical meridians, and their only differences is in the spacing between parallels. Although the orthographical projection appears to preserve the

bearing from the center to all outer points, they cannot preserve such bearing. Therefore, we can imagine that these projections will entail map projection error.

There are two notes that will be of use in our succeeding analysis. First, the three projections show any great circle on the Northern Hemisphere as a concave downward curve, like the great circle arcs between Tokyo and Hawaii in Figures 1, 2 and 3. Second, both on the equirectangular and equal-area projections, the Tissot's indicatrices are given by circles if and only if they are located on the standard parallels. This can be confirmed in Figures 2 and 3. The proof of these two notes are given in Appendix A.1.

2.3. Numerical Examples

We shall examine numerically how the planar solutions differ from the spherical one by using the following three data sets: (d1) national data in the European Union (EU); (d2) state data in the United States (US); and (d3) prefectural data in Japan. In the first data set, we use the locations of the capitals of 15 nations as the demand points and their national populations as their weights. Similarly, in the second (third) data, we use the capitals of 51 states (47 prefectures) as the demand points and the population of their states (prefectures) as their weights. Note that these three data sets fulfill assumption (a1) made in Section 2.1.

For each data set, first we find out the spherical solutions by using standard iterative solution procedure: see Drezner and Wesolowsky (1978), Love et al.(1988). Fortunately, no absorbed cases occur, indicating that these data sets meet assumption (a2). Second, we compute planar solutions on the three types of map projections by means of common iterative solution method: see Love et al.(1988). Under equirectangular and equal-area projections, the standard parallels range from 0° to 80° at 10° intervals. Third, we calculate the great circle distances in *km* between the spherical and planar solutions as location errors.

All the computational results are provided in Tables 1, 2 and 3, where θ indicates the latitudes of the standard parallels. Bold figures in the coordinate of latitude represent that planar solutions are located on the south of the corresponding spherical solution. These tables reveal that many planar solutions are located on the south of the spherical solution, although choice of maps and standard lines affects more or less these planar solutions. More precisely two observations can been defined.

(c1) the geographical tendency necessariiy holds if we choose Mercator projection, or equirectangular or equal-area projections with standard parallels near the demand data; and

(c2) the geographical tendency more frequently holds for the EU's and US's data sets than Japan' one.

The EU's and US's data sets differ geographically from that of Japan's in three respects:

(g1) the EU's and US's data distributed more symmetrically than Japan's data set;

(g2) the US's data set has the widest distribution among the three data sets; and

(g3) the EU's data set is located most northerly among the three data sets.

The second observation will be explained theoretically based on the three abovementioned geographical points.

3. THEORETICAL RESULTS

3.1. Interpretation of the first observation

Figure 5 presents the locations of the fifteen capitals in the EU on Mercator projection map. Figure 6 expresses the locations on the orthographic projection centered on its spherical solution. In these figures, the locations are indicated by • and ∘, respectively. They are also connected with the spherical solution, denoted by ⊙, by great circle arcs. Figure 7 shows the two types of locations for these capitals obtained by merging Figures 5 and 6 in such a way that the locations of the spherical solution on Figure 5 and Figure 6 coincide. We see from Figure 7 that each great circle arc on the orghographic projection always lies above the corresponding great circle arc on the Mercator projection. Thus, we would expect that inequality (5) to hold.

Property 1 *Under Mercator projection, or under equirectangular or equal-area projections with the standard parallel fixed at ϕ^*th parallels,* $\frac{\partial PW(\mathbf{p}:S)}{\partial y}|_{\mathbf{p}=\mathbf{p}^*} > 0$.

See Appendix A.2 for derivation of this property. On equirectangular or equal-area projections, the distortions of scale and shape characteristics are pretty small in a narrow region near the standard parallels because these projections preserve the distances on that parallel. Therefore, it is natural for decision-makers in actual facility planning to choose maps with a standard parallel near the demand set as much as possible from a practical point of view.

Property 1 can be intuitively interpreted as follows. There is no angular deformation at the spherical solution on these projections, as seen in Section 2.2. In addition, any great circle on the Northern Hemisphere is represented by a concave downward curve, as pointed out in the said section. Combining these two results gives that they underestimate all bearings since

the orthographic projection preserves bearing.

On the other hand, if the standard parallel is set more south (resp. north) than the spherical solution, then the length of the parallel where the spherical solution lies will be too long (resp. too short), as compared to that of meridians. This implies that the image of great circle arcs starting from the spherical solution in the south (resp. north) direction can be above in its neighborhood than that on the orthographic projection centered on it. This can be confirmed in the shapes of Tissot's indicatrices in Figures 2 and 3.

3.2. Interpretation of the second observation from the first geographical point of view

We call the demand set S *symmetric* if the demand set S consists of an even number of equal-weighted demand points with $n = 2k(k \geq 1)$ and there exists a spherical point $\mathbf{p}_0$ in such a way that the great circle arc between $\mathbf{p}_i$ and $\mathbf{p}_{k+i}$ passes $\mathbf{p}_0$ for every $i(1 \leq i \leq k)$. An example of a symmetric demand data is four demand points with the same weight on the vertices of a quadrilateral. Another examples are the sets wherein each member is located at all the vertices of spherical regular n-gons for even n. It is evident from the definition of the symmetric set that $\mathbf{p}_0$ is a spherical solution.

Since the line connecting the planar images $f(\mathbf{p}_i)$ and $f(\mathbf{p}_{k+i})$ is concave upward, it crosses the prime meridian at a southern parallel than $f(\mathbf{p}^*)$ for every $i(1 \leq i \leq k)$. Hence, we can expect that inequality $\frac{\partial PW(\mathbf{p};S)}{\partial y}|_{\mathbf{p}=\mathbf{p}^*} > 0$ holds.

Property 2 *If S is symmetric, then inequality $\frac{\partial PW(\mathbf{p};S)}{\partial y}|_{\mathbf{p}=\mathbf{p}^*} > 0$ holds under equirectangular or equal-area projections with any standard parallel.*

Thus, Property 2 may give a justification for the second observation theoretically.

3.3. Interpretation of the second observation from the second geographical point of view

If a projection shows a great circle arc on the Northern Hemisphere as a concave curve, then it further underestimates actual bearing as the point is farther from a starting point along the arc. Therefore, we would expect that inequality $\frac{\partial PW(\mathbf{p};S)}{\partial y}|_{\mathbf{p}=\mathbf{p}^*} > 0$ holds, when the demand points are widely distributed.

For the demand set S, consider another set $\acute{S} \equiv \{\acute{\mathbf{p}}_1, \acute{\mathbf{p}}_2, \cdots, \acute{\mathbf{p}}_n\}$ on the spherical surface that is generated by extending $\mathbf{p}_i$ outwards from the spherical solution $\mathbf{p}^*$ along the great circle through $\mathbf{p}^*$ and $\mathbf{p}_i$. Let $\alpha(\mathbf{p}^*, \mathbf{p}_i)$ be the bearing from $\mathbf{p}^*$ to $\mathbf{p}_i$. Mathematically, for a fixed dilatation rate $\Delta(\geq 1)$, $\acute{S}$ is uniquely determined such that $\delta(\mathbf{p}^*, \acute{\mathbf{p}}_i) = \Delta\delta(\mathbf{p}^*, \mathbf{p}_i)$ and

$\alpha(\mathbf{p}^*, \acute{\mathbf{p}}_i) = \alpha(\mathbf{p}^*, \mathbf{p}_i)$ for all $i \in I$. Since the set $\acute{S}$ is similar to the original demand set S, $\mathbf{p}^*$ is also a spherical solution for the demand set $\acute{S}$.

Property 3 *As the dilatation rate Δ increases, so does $\frac{\partial PW(\mathbf{p}:\acute{S})}{\partial y}|_{\mathbf{p}=\mathbf{p}^*}$ under equirectangular or equal-area projections, regardless of standard parallels, provided that all the $\acute{\mathbf{p}}_i$'s exist on the Northern Hemisphere.*

The proof is provided in Appendix A.3. This property cannot necessarily ensure $\frac{\partial PW(\mathbf{p}:\acute{S})}{\partial y}|_{\mathbf{p}=\mathbf{p}^*} > 0$. However, we can expect this inequality to hold as the demand points are more widely distributed over a large region of the surface. Thus, Property 3 may give an explanation for the second observation.

3.4. Interpretation of the second observation from the third geographical point of view

Although the image of the great circle arc starting from a point in the south direction under any cylindrical projection always goes down, the image under the orthographic projection centered on the point may go up. This can be seen in Figure 4, where the planar image of the great circle arcs from Tokyo to Hawaii goes up. In addition, as the demand points are situated toward the North Pole, this contrast becomes more remarkable, indicating that inequalities $\frac{\partial PW(\mathbf{p}:\acute{S})}{\partial y}|_{\mathbf{p}=\mathbf{p}^*} > 0$ may hold through inequality (5).

For the demand set S, consider another set $\hat{S} \equiv \{\hat{\mathbf{p}}_1, \hat{\mathbf{p}}_2, \cdots, \hat{\mathbf{p}}_n\}$ on the surface of a sphere that is generated by rotating $\mathbf{p}_i$'s northward around the axis through two spherical points $\{-\pi/2, 0\}$ and $\{\pi/2, 0\}$. Mathematically, for a given rotation angle $\Phi(\geq 0)$, $\hat{S}$ is uniquely determined such that $\hat{\mathbf{p}}^* \equiv \{\phi^* + \Phi, 0\}$, $\alpha(\hat{\mathbf{p}}^*, \hat{\mathbf{p}}_i) = \alpha(\mathbf{p}^*, \mathbf{p}_i)$ and $\delta(\hat{\mathbf{p}}^*, \hat{\mathbf{p}}_i) = \delta(\mathbf{p}^*, \mathbf{p}_i)$ for all $i \in I$. Thus, $\mathbf{p}^*$ is rotated along the prime meridian through Φ, while both its distance and bearing to $\mathbf{p}_i$'s are kept fixed. Since the set $\hat{S}$ is geometrically congruent to the original data set S, $\hat{\mathbf{p}}^*$ is a spherical solution for the demand set $\hat{S}$. Divide the set S into $\hat{S}^+$ and $\hat{S}^-$, where $\hat{S}^+ \equiv \{\hat{\mathbf{p}}_i | f_y(\hat{\mathbf{p}}_i) > \phi^* + \Phi\}$ and $\hat{S}^- \equiv \{\hat{\mathbf{p}}_i | f_y(\hat{\mathbf{p}}_i) \leq \phi^* + \Phi\}$. Note that $\frac{\partial PW(\mathbf{p}:\hat{S})}{\partial y} = \frac{\partial PW(\mathbf{p}:\hat{S}^+)}{\partial y} + \frac{\partial PW(\mathbf{p}:\hat{S}^-)}{\partial y}$, $\frac{\partial PW(\mathbf{p}:\hat{S}^+)}{\partial y}|_{\mathbf{p}=\mathbf{p}^*} < 0$ and $\frac{\partial PW(\mathbf{p}:\hat{S}^-)}{\partial y}|_{\mathbf{p}=\mathbf{p}^*} \geq 0$.

Property 4 *As the rotation angle Φ increases, both under equirectangular or equal-area projections, 1) the number of the members within $\hat{S}^+$ decreases and 2) $\frac{\partial PW(\mathbf{p}:\hat{S}^+)}{\partial y}|_{\mathbf{p}=\mathbf{p}^*}$ increases, regardless of standard parallels, provided that all the $\hat{\mathbf{p}}_i$'s exist on the Northern Hemisphere.*

The proof is given in Appendix A.4. This property does not necessarily ensure $\frac{\partial PW(\mathbf{p}:\hat{S})}{\partial y}|_{\mathbf{p}=\mathbf{p}^*} > 0$ because $\frac{\partial PW(\mathbf{p}:\hat{S}^-)}{\partial y}|_{\mathbf{p}=\mathbf{p}^*}$ may decrease with Φ. However, since we can expect the inequality

to hold as the demand set is located toward more north, Property 4 can give a reason for the second observation.

3.5. Other cylindrical map projections

The projection errors on other cylindrical projections will be examined. Under Gall's stereographic projection, the image of $\mathbf{p} = (\phi, \lambda)$ is given by $(\lambda, 2\tan(\phi/2))$. Its planar coordinate under Miller cylindrical projection is given by $(\lambda, (5/4)\ln[\tan(\pi/4 + 2\phi/5)])$. These transformation equations, which can be found in Bugayeuskiy and Snyder(1995), resemble the Mercator projection. Any great circle in the Northern Hemisphere under these projections appears as a concave downward curve, as demonstrated in Appendix A.1. Therefore, Properties 2 and 3 hold for these two cylindrical projections. As shown in Snyder(1993), central cylindrical projection transforms $\mathbf{p}$ into $(\lambda, \tan\phi)$. Distortion becomes increasingly extreme near the polar regions, so it has been rarely used for pratical purposes, and it can not show all great circles as concave downward curves. Therefore, we see that Properties 2 and 3 cannot be applied to all cylindrical projections.

Property 4 can be applied to cylindrical projections where the spacing between parallels is more compressed with their latitudes.

In conclusion, we see that our findings are applicable to many other cylindrical projections.

4. CONCLUSIONS

This paper has analyzed how cylindrical conformal, equidistant, and equal-area map projection introduce errors in planar Weber problems. It makes at least two principal contributions. Firstly, it showed that most planar solutions are located on the south of the spherical solution. This geographical tendency was inclined to hold as the demand points were distributed widely or symmetrically or toward the north. Secondly, it demonstrated that this geographical tendency is always present if we choose Mercator projection, or equirectangular or equal-area projections with standard parallels placed at the latitude of the spherical Weber solution.

We have assumed in this paper that all demand points are located on the Northern Hemisphere. It is clear, however, that based on symmetry the same story holds if demand points are located on the Southern Hemisphere.

Acknowledgement

This paper was partially written while the first author was visiting the Department of Geography at the Catholic University of Louvain, Louvain-la-Neuve, Belgium from 1993 to 1994. He is grateful for the hospitality of this department. An earlier version of this paper was presented in 1994 at the Seventh Meeting of the European Operational Research Working Group on Locational Analysis in Brussels, and in 1996 at the Fifth World Congress of the Regional Science Association International in Tokyo. The author would also like to thank the participants as well as Hirofumi Kagaya for their valuable comments.

References

[1] Boltyanski, V., Martini, H. and Soltan, V.(1999): *Geometric methods and optimization problems*, Kluwer Academic Publishers, Dordrecht.

[2] Bugayeuskiy, L.M. and Snyder, J.P.(1995): *Map projections.* Taylor and Francis, Philadelphia.

[3] Drezner, Z. and Wesolowsky, G.O.(1978): Facility location on a sphere, *Journal of the Operational Research Society, 29*, 997-1004.

[4] Hansen, P., Jaumard, B. and Krau, S.(1995): An algorithm for Weber's problem on the sphere, *Location Science, 3*, 217-237. *6*, 175-196.

[5] Litwhiler, D.W. and Aly, A.A.(1979): Large region location problems, *Computers and Operations Research, 6*, 1-12.

[6] Litwhiler, D.W. and Aly, A.A.(1980): Steiner's problem and Fagnano's result on the sphere, *Mathematical Programming, 18*, 286-290.

[7] Love, R.F., Morris, J.G. and Wesolowsky,G.O.(1988): *Facilities location.* North-Holland, New York.

[8] McDonnell, P.W.(1979): *Introduction to map projection.* Marcel Dekker, New York.

[9] Snyder, J.P.(1993): *Flattening the earth.* University of Chicago Press, Chicago.

[10] Xue, G.-L.(1994): A globally convergent algorithm for facility location on a sphere, *Computers and Mathematics with Applications, 27*, 37-50.

MATHEMATICAL APPENDIX

A.1. Proof of two notes in Sections 2.2

In order to prove the first note, it suffices to show that $\frac{d^2 f_y(\mathbf{p})}{df_x(\mathbf{p})^2} < 0$ for any point $\mathbf{p} \equiv \{\phi, \lambda\}$ on the great circle arc between $\mathbf{p}^*$ and $\mathbf{p}_i$. Assume that $\lambda_i > 0$ and obtain $\lambda_i < 0$ by symmetry. Let T_O be the tangent of the counterclockwise angle from the positive x-axis to the vector from the planar locations $\mathbf{g}(\mathbf{p}^*)$ to $\mathbf{g}(\mathbf{p}_i)$ under the orthographic projection centered on $\mathbf{p}^*$. Its transformation (4) implies

$$T_O \equiv \frac{g_y(\mathbf{p}_i) - g_y(\mathbf{p}^*)}{g_x(\mathbf{p}_i) - g_x(\mathbf{p}^*)} = \frac{\sin\phi^* \cos\phi_i[1 - \cos\lambda_i] + \sin(\phi_i - \phi^*)}{\sin\lambda_i \cos\phi_i}.$$

Since the orthographical projection centered on $\mathbf{p}^*$ preserves bearing from $\mathbf{p}^*$ to $\mathbf{p}$, we get

$$\frac{\sin\phi^* \cos\phi[1 - \cos\lambda] + \sin(\phi - \phi^*)}{\sin\lambda \cos\phi} = T_O.$$

Hence, ϕ can be explicitly expressed with respect to λ as follows:

$$\phi = \arctan[h(\lambda)], \tag{6}$$

where $h(\lambda) \equiv \tan\phi^* \sqrt{1 + (T_O/\sin\phi^*)^2} \sin\left(\lambda + \arcsin \frac{1}{\sqrt{1+(T_O/\sin\phi^*)^2}}\right)$. Straightforward manipulation, while noting $h(\lambda)'' = h(\lambda)$, yields

$$\frac{d\phi}{d\lambda} = \frac{h(\lambda)'}{1 + h(\lambda)^2} \qquad \frac{d^2\phi}{d\lambda^2} = -\frac{h(\lambda)}{1 + h(\lambda)^2}\left(1 + 2\frac{(h(\lambda)')^2}{1 + h(\lambda)^2}\right). \tag{7}$$

Differentiating $f_y(\mathbf{p})$ with respect to $f_x(\mathbf{p})$, while noting $\frac{d^2\lambda}{df_x(\mathbf{p})^2} = 0$ for the projections to be considered in this paper, and using (6) and (7), yields

$$\begin{aligned}
\frac{df_y(\mathbf{p})}{df_x(\mathbf{p})} &= \frac{df_y(\mathbf{p})}{d\phi}\frac{d\phi}{d\lambda}\frac{d\lambda}{df_x(\mathbf{p})}, \\
\frac{d^2 f_y(\mathbf{p})}{df_x(\mathbf{p})^2} &= \left[\left(\frac{d^2 f_y(\mathbf{p})}{d\phi^2} - 2\tan\phi\frac{df_y(\mathbf{p})}{d\phi}\right)\left(\frac{d\phi}{d\lambda}\right)^2 - \tan\phi\frac{df_y(\mathbf{p})}{d\phi}\right]\left(\frac{d\lambda}{df_x(\mathbf{p})}\right).
\end{aligned}$$

In order to show that the sign of this second derivative is always negative for all permissible values of ϕ, it suffices to prove that 1) $\frac{df_y(\mathbf{p})}{d\phi} > 0$ and; 2) $\Delta \equiv \frac{d^2 f_y(\mathbf{p})}{d\phi^2} - 2\tan\phi\frac{df_y(\mathbf{p})}{d\phi} < 0$ because $\frac{d\lambda}{df_x(\mathbf{p})} > 0$ for the projections.

If we use the equirectangular projection, then $\frac{df_y(\mathbf{p})}{d\phi} = \sec\theta > 0$ and $\frac{d^2 f_y(\mathbf{p})}{d\phi^2} = 0$, indicating that $\Delta > 0$. When we adopt the equal-area projection, then $\frac{df_y(\mathbf{p})}{d\phi} = \cos\phi/\cos\theta > 0$ and $\frac{d^2 f_y(\mathbf{p})}{d\phi^2} = -\sin\phi/\cos\theta < 0$, indicating that $\Delta > 0$. For the Mercator projection, $\frac{df_y(\mathbf{p})}{d\phi} = \sec\phi > 0$ and $\frac{d^2 f_y(\mathbf{p})}{d\phi^2} = \tan\phi\sec\phi$, leading to $\Delta = -\tan\phi\sec\phi < 0$. In the case

of the Gall projection, $\frac{\mathrm{d}f_y(\mathbf{p})}{\mathrm{d}\phi} = \sec^2(\phi/2) > 0$ and $\frac{\mathrm{d}^2 f_y(\mathbf{p})}{\mathrm{d}\phi^2} = \tan(\phi/2)\sec^2(\phi/2)$, showing $\Delta = \sec^2(\phi/2)(\tan(\phi/2) - 2\tan\phi) < 0$. When we use the Miller projection, then $\frac{\mathrm{d}f_y(\mathbf{p})}{\mathrm{d}\phi} = \sec(4\phi/5) > 0$ and $\frac{\mathrm{d}^2 f_y(\mathbf{p})}{\mathrm{d}\phi^2} = (4/5)\tan(4\phi/5)\sec(4\phi/5)$, indicating that $\Delta = \sec^2(4\phi/5)\left((4/5)\sin(4\phi/5) - 2\tan\phi\cos(4\phi/5)\right) \leq -\sec^2(4\phi/5)\sin\phi < 0$.

Next, let us prove the second note. Under Mercator or under the equirectangular projections with the standard parallel fixed at ϕ^*th parallels, $\frac{\mathrm{d}f_y(\mathbf{p})}{\mathrm{d}\phi} = \sec\phi^*$ and $\frac{\mathrm{d}\lambda}{\mathrm{d}f_x(\mathbf{p})} = 1$. On the other hand, under equal-area projection with the standard parallel fixed at ϕ^*th parallels, $\frac{\mathrm{d}f_y(\mathbf{p})}{\mathrm{d}\phi} = 1$ and $\frac{\mathrm{d}\lambda}{\mathrm{d}f_x(\mathbf{p})} = \sec\phi^*$. Accordingly, while using the first in (7), we obtain

$$\frac{\mathrm{d}f_y(\mathbf{p})}{\mathrm{d}f_x(\mathbf{p})}\Big|_{\mathbf{p}=\mathbf{p}^*} = \frac{\mathrm{d}f_y(\mathbf{p})}{\mathrm{d}\phi}\frac{\mathrm{d}\phi}{\mathrm{d}\lambda}\frac{\mathrm{d}\lambda}{\mathrm{d}f_x(\mathbf{p})}\Big|_{\lambda=0} = \sec\phi^*\left(\frac{1}{1+\tan^2\phi^*}\frac{T_O}{\cos\phi^*}\right) = T_O,$$

as required. □

A.2. Proof of Property 1

Denote $T(\mathbf{p}_i)$ as

$$T(\mathbf{p}_i) = \frac{f_y(\mathbf{p}_i) - f_y(\mathbf{p}^*)}{f_x(\mathbf{p}_i) - f_x(\mathbf{p}^*)}.$$

Since the image of a great circle arc is concave downward, we get $T(\mathbf{p}_i) \leq \frac{\mathrm{d}f_y(\mathbf{p})}{\mathrm{d}f_x(\mathbf{p})} = T_O$. This implies $\frac{f_y(\mathbf{p}_i)-f_y(\mathbf{p}^*)}{d(\mathbf{f}(\mathbf{p}_i),\mathbf{f}(\mathbf{p}^*))} < \frac{g_y(\mathbf{p}_i)-g_y(\mathbf{p}^*)}{d(\mathbf{g}(\mathbf{p}_i),\mathbf{g}(\mathbf{p}^*))}$, so we obtain inequalities (5), as required. □

A.3. Proof of Property 3

For any point $\mathbf{p} \equiv \{\phi, \lambda\}$ on the great circle through $\mathbf{p}^*$ and $\mathbf{p}_i$ with $\lambda_i > 0$, $\frac{\mathrm{d}f_x(\mathbf{p})}{\mathrm{d}\Delta} > 0$ because of cylindrical projections. On the other hand, from the definition of $T(\mathbf{p})$, it is easy to check that

$$\frac{\mathrm{d}T(\mathbf{p})}{\mathrm{d}f_x(\mathbf{p})} = \frac{1}{(f_x(\mathbf{p}) - f_x(\mathbf{p}^*))^2}\left(f_x(\mathbf{p})\frac{\mathrm{d}f_y(\mathbf{p})}{\mathrm{d}f_x(\mathbf{p})} - (f_y(\mathbf{p}) - f_y(\mathbf{p}^*))\right).$$

For $z(\lambda) \equiv f_x(\mathbf{p})\frac{\mathrm{d}f_y(\mathbf{p})}{\mathrm{d}f_x(\mathbf{p})} - (f_y(\mathbf{p}) - f_y(\mathbf{p}^*))$, one can easily verify that $z(0) = 0$, and $\frac{\mathrm{d}z(\lambda)}{\mathrm{d}\lambda} = f_x(\mathbf{p})\frac{\mathrm{d}^2 f_y(\mathbf{p})}{\mathrm{d}f_x(\mathbf{p})^2} < 0$ because of the proof of Appendix A.1. Hence, we get $z(\lambda) < 0$ for $\forall\lambda > 0$, so $\frac{\mathrm{d}T(\mathbf{p})}{\mathrm{d}\lambda} < 0$. Combining these two results yields $\frac{\mathrm{d}T(\mathbf{p})}{\mathrm{d}\Delta} = \frac{\mathrm{d}T(\mathbf{p})}{\mathrm{d}f_x(\mathbf{p})}\frac{\mathrm{d}f_x(\mathbf{p})}{\mathrm{d}\Delta} < 0$, so we obtain $\frac{f_y(\mathbf{p}'_i)-f_y(\mathbf{p}^*)}{d(\mathbf{f}(\mathbf{p}'_i),\mathbf{f}(\mathbf{p}^*))}$ decreases with Δ, as required. □

A.4. Proof of Property 4

Denote C_1 and C_2 as $C_1 \equiv \cos\phi^*\cos\phi_i\cos\lambda_i + \sin\phi^*\sin\phi_i$ and $C_2 \equiv \sin\lambda_i\cos\phi_i$. For

$\hat{\mathbf{p}}_i \equiv (\phi, \lambda)$, once Φ is given, combining $\delta(\hat{\mathbf{p}}, \hat{\mathbf{p}}^*) = \delta(\mathbf{p}_i, \mathbf{p}^*)$ together with $\alpha(\hat{\mathbf{p}}, \hat{\mathbf{p}}^*) = \alpha(\mathbf{p}_i, \mathbf{p}^*)$ yields the following simultaneous system of equations with respect to ϕ and λ:

$$\cos(\phi^* + \Phi)\cos\phi\cos\lambda + \sin(\phi^* + \Phi)\sin\phi = C_1, \qquad \sin\lambda\cos\phi = C_2. \tag{8}$$

Eliminating λ in this system yields

$$\phi^* + \Phi = \arcsin(\sin\phi/\sqrt{1 - C_2^2}) + \arccos(C_1/(1 - C_2^2)).$$

Differentiating Φ with respect to ϕ yields $\frac{\mathrm{d}\Phi}{\mathrm{d}\phi} = \frac{\cos\phi}{\sqrt{\cos^2\phi - C_2^2}} = \frac{1}{\cos\lambda}$. Applying the inverse-function rule of differential calculus leads to

$$\frac{\mathrm{d}\phi}{\mathrm{d}\Phi} = \cos\lambda. \tag{9}$$

On the other hand, rewriting the second equation in (8) yields $\lambda = \arcsin(C_2/\cos\phi)$. Differentiating this with respect to ϕ yields $\frac{\mathrm{d}\lambda}{\mathrm{d}\phi} = \tan\lambda\tan\phi$. This together with (9) yields

$$\frac{\mathrm{d}\lambda}{\mathrm{d}\Phi} = \frac{\mathrm{d}\lambda}{\mathrm{d}\phi}\frac{\mathrm{d}\phi}{\mathrm{d}\Phi} = \sin\lambda\tan\phi > 0. \tag{10}$$

For $\mathbf{p}_i$ with $\lambda_i > 0$, let $\hat{T}(\hat{\mathbf{p}}_i)$ be $\hat{T}(\hat{\mathbf{p}}) = \frac{f_y(\hat{\mathbf{p}}) - f_y(\hat{\mathbf{p}}^*)}{f_x(\hat{\mathbf{p}}) - f_x(\hat{\mathbf{p}}^*)}$. Differentiating $\hat{T}(\hat{\mathbf{p}})$ with respect to Φ yields

$$\frac{\mathrm{d}\hat{T}(\hat{\mathbf{p}})}{\mathrm{d}\Phi} = \frac{1}{f_x(\hat{\mathbf{p}}) - f_x(\hat{\mathbf{p}}^*)}\left[\left(\frac{\mathrm{d}f_y(\hat{\mathbf{p}}) - f_y(\hat{\mathbf{p}}^*)}{\mathrm{d}\Phi}\right) - \hat{T}(\hat{\mathbf{p}})\left(\frac{\mathrm{d}f_x(\hat{\mathbf{p}}) - f_x(\hat{\mathbf{p}}^*)}{\mathrm{d}\Phi}\right)\right].$$

Using (9) yields

$$\frac{\mathrm{d}f_y(\hat{\mathbf{p}}) - f_y(\hat{\mathbf{p}}^*)}{\mathrm{d}\Phi} = \frac{\mathrm{d}f_y(\hat{\mathbf{p}})}{\mathrm{d}\phi}\frac{\mathrm{d}\phi}{\mathrm{d}\Phi} - \frac{\mathrm{d}f_y(\hat{\mathbf{p}})}{\mathrm{d}\phi}\frac{\mathrm{d}\phi}{\mathrm{d}\Phi}|_{\lambda=0} = \cos\lambda\frac{\mathrm{d}f_y(\hat{\mathbf{p}})}{\mathrm{d}\phi} - \frac{\mathrm{d}f_y(\hat{\mathbf{p}})}{\mathrm{d}\phi}|_{\phi=\phi^*+\Phi} \leq 0,$$

where the last inequality holds since $\frac{\mathrm{d}^2 f_y(\hat{\mathbf{p}})}{\mathrm{d}\phi^2} \leq 0$ for the equirectangular and equal-area projections, and $f_y(\hat{\mathbf{p}}_i) > f_y(\hat{\mathbf{p}}^*)$, *i.e.*, $\phi > \phi^* + \Phi$. Similarly, using (10) gives

$$\frac{\mathrm{d}f_x(\hat{\mathbf{p}}) - f_x(\hat{\mathbf{p}}^*)}{\mathrm{d}\Phi} = \frac{\mathrm{d}f_x(\hat{\mathbf{p}})}{\mathrm{d}\lambda}\frac{\mathrm{d}\lambda}{\mathrm{d}\Phi} - \frac{\mathrm{d}f_x(\hat{\mathbf{p}})}{\mathrm{d}\lambda}\frac{\mathrm{d}\lambda}{\mathrm{d}\Phi}|_{\lambda=0} = \sin\lambda\tan\phi\frac{\mathrm{d}f_x(\hat{\mathbf{p}})}{\mathrm{d}\lambda} > 0,$$

where the last inequality holds since $\frac{\mathrm{d}f_x(\hat{\mathbf{p}})}{\mathrm{d}\lambda} > 0$ for cylindrical projections. Since $f_x(\hat{\mathbf{p}}) > f_x(\hat{\mathbf{p}}^*)$ for cylindrical projections, and $\hat{T}(\hat{\mathbf{p}}) > 0$ for $\phi > \phi^* + \Phi$, we obtain $\frac{\mathrm{d}\hat{T}(\hat{\mathbf{p}}_i)}{\mathrm{d}\Phi} < 0$. This indicates that $|\hat{S^+}|$ decreases and $\frac{\partial PW(\mathbf{p};\hat{S^+})}{\partial y}$ increases with Φ, as required. □

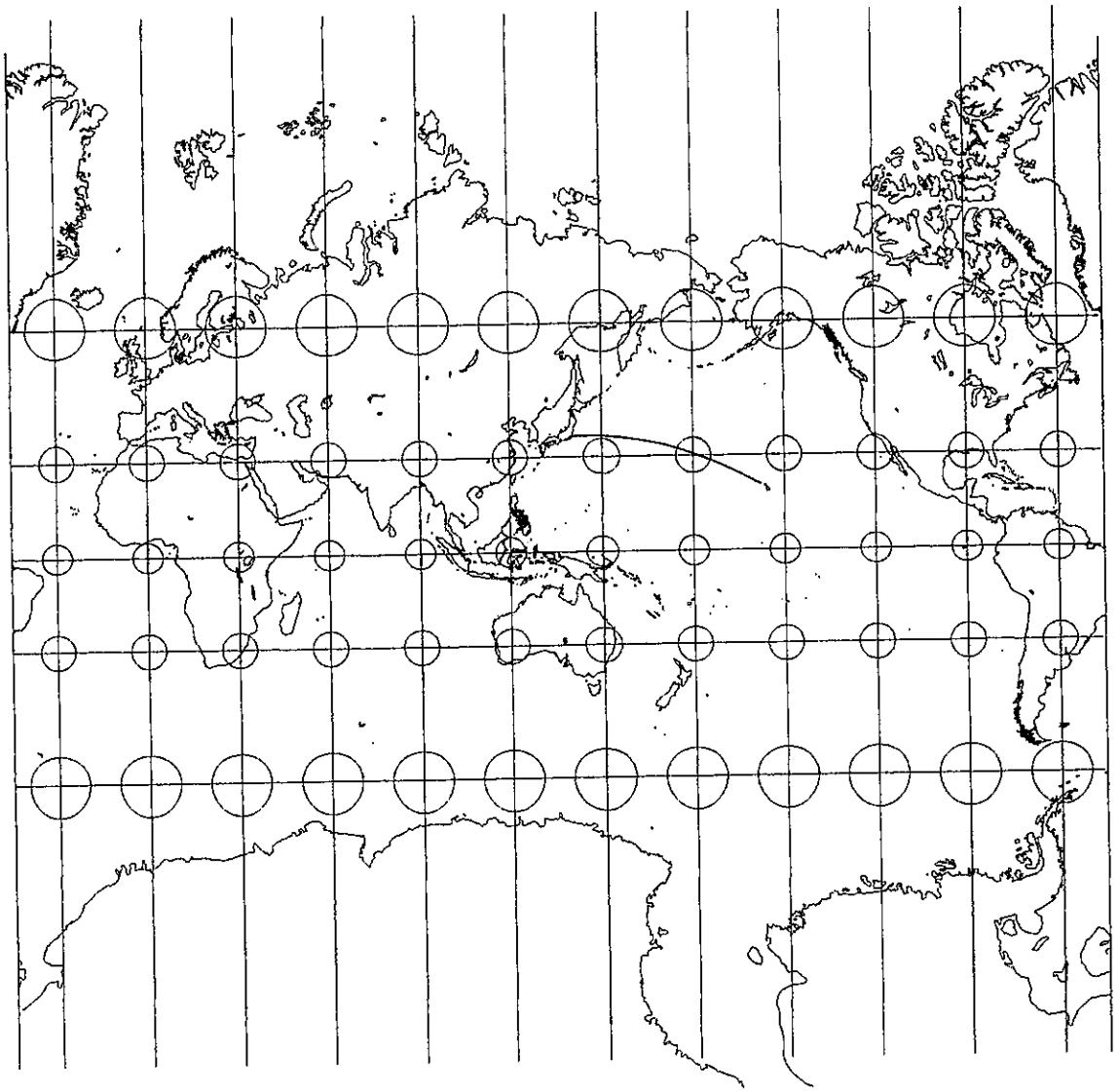

Figure 1: World map on Mercator projection

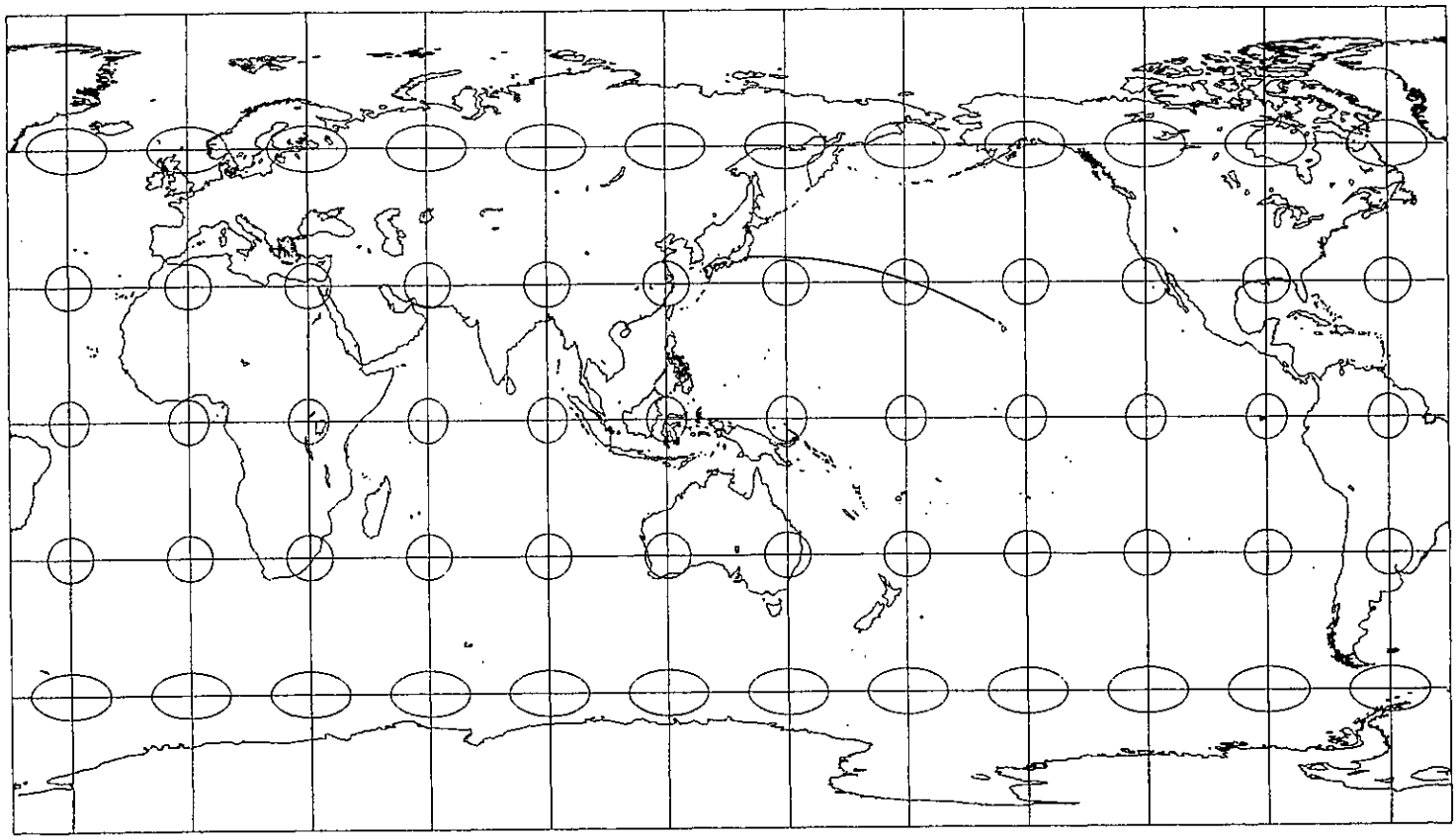

Figure 2: World map on equirectangular projection with standard parallels at 30°

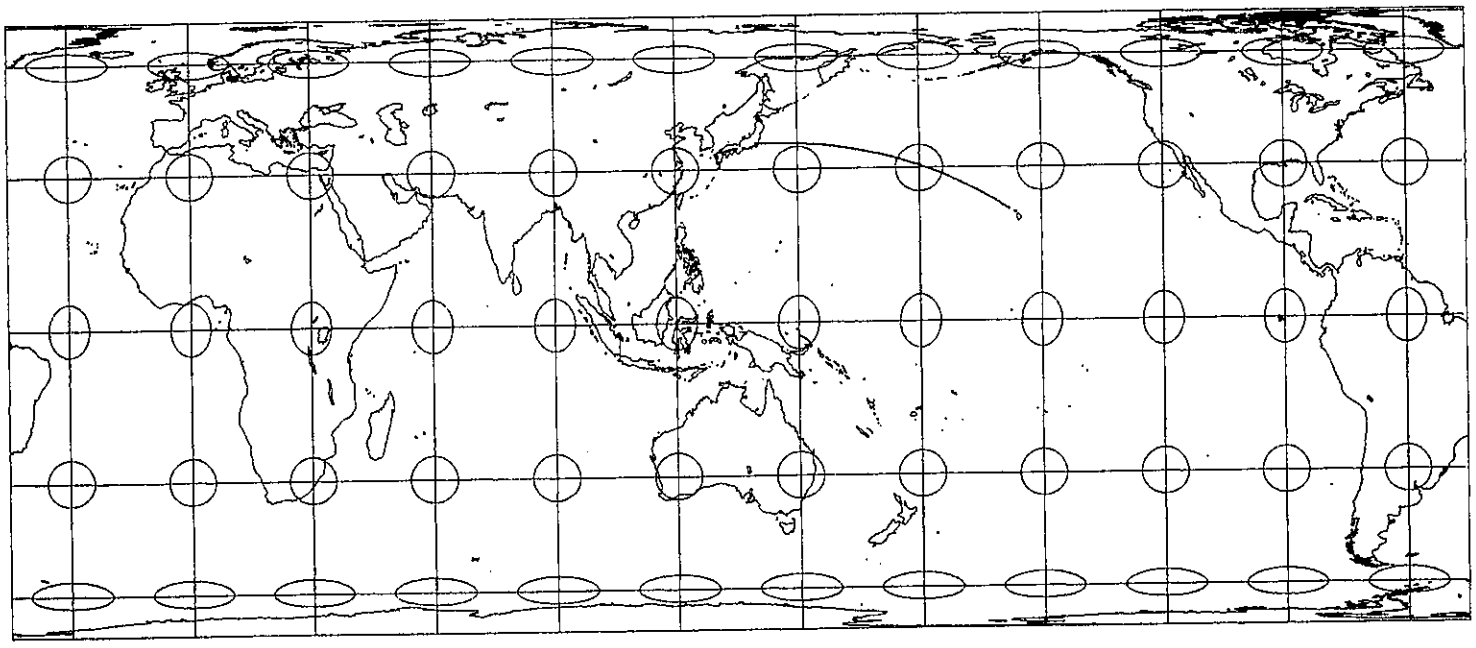

Figure 3: World map on equal-area projection with standard parallels at 30°

Figure 4: Hemisphere map on orthographic projection centered on Tokyo.

Figure 5: European map on Mercator projection

Figure 6: European map on an orthographic projection centered on its spherical solution

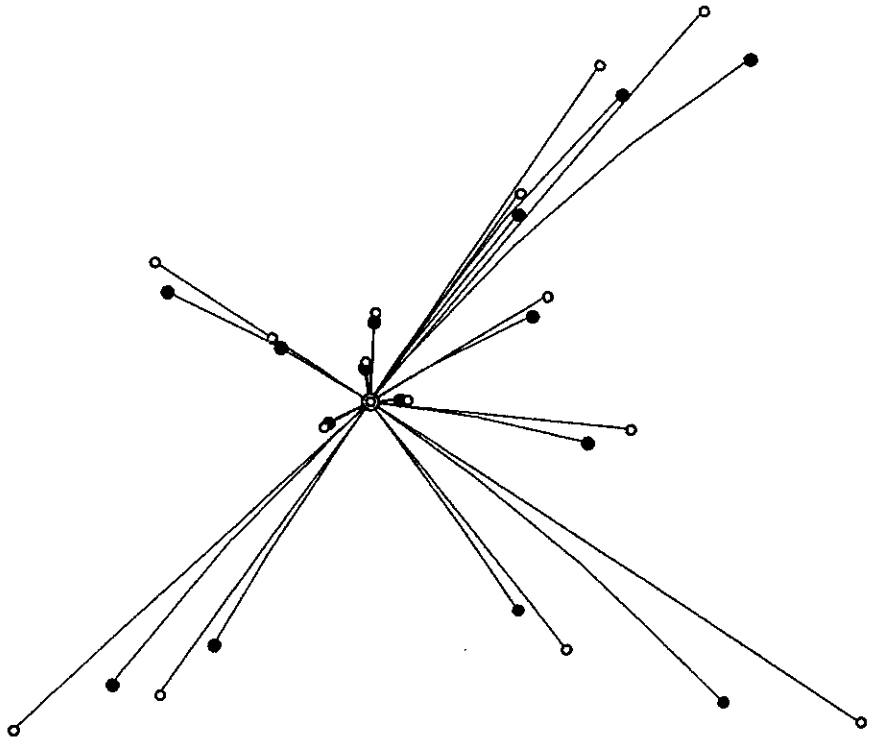

Figure 7: Comparison of planar locations of capitals

Table 1: Weber solutions and location errors using European data

			latitude-longitude coordinate		location error
spherical solution			*49 ° 38 ′ N*	*4 ° 37 ′ E*	-
planar solution	Mercator		**49 ° 25 ′ N**	4 ° 36 ′ E	25.0
	equirectangular	$\theta = 0$	**49 ° 17 ′ N**	4 ° 47 ′ E	40.7
		10	**49 ° 17 ′ N**	4 ° 46 ′ E	40.5
		20	**49 ° 17 ′ N**	4 ° 45 ′ E	40.0
		30	**49 ° 18 ′ N**	4 ° 43 ′ E	38.8
		40	**49 ° 18 ′ N**	4 ° 40 ′ E	36.8
		50	**49 ° 20 ′ N**	4 ° 36 ′ E	33.8
		60	**49 ° 23 ′ N**	4 ° 31 ′ E	29.5
		70	**49 ° 28 ′ N**	4 ° 31 ′ E	20.6
		80	49 ° 42 ′ N	4 ° 49 ′ E	16.3
	equal-area	$\theta = 0$	**49 ° 11 ′ N**	4 ° 54 ′ E	54.4
		10	**49 ° 11 ′ N**	4 ° 54 ′ E	54.8
		20	**49 ° 10 ′ N**	4 ° 53 ′ E	55.6
		30	**49 ° 10 ′ N**	4 ° 51 ′ E	55.2
		40	**49 ° 11 ′ N**	4 ° 45 ′ E	50.8
		50	**49 ° 16 ′ N**	4 ° 35 ′ E	41.9
		60	**49 ° 23 ′ N**	4 ° 28 ′ E	30.2
		70	49 ° 38 ′ N	4 ° 47 ′ E	12.1
		80	50 ° 43 ′ N	4 ° 44 ′ E	120.7

Table 2: Weber solutions and location errors using American data

			latitude-longitude coordinate		location error
spherical solution			*38 ° 57 ′ N*	*87 ° 33 ′ W*	-
planar solution	Mercator		**38 ° 16 ′ N**	87 ° 33 ′ W	77.1
	equirectangular	$\theta = 0$	**38 ° 02 ′ N**	87 ° 28 ′ W	103.7
		10	**38 ° 02 ′ N**	87 ° 28 ′ W	102.5
		20	**38 ° 04 ′ N**	87 ° 29 ′ W	98.8
		30	**38 ° 08 ′ N**	87 ° 31 ′ W	92.4
		40	**38 ° 13 ′ N**	87 ° 33 ′ W	82.8
		50	**38 ° 20 ′ N**	87 ° 35 ′ W	69.2
		60	**38 ° 30 ′ N**	87 ° 39 ′ W	50.6
		70	**38 ° 45 ′ N**	87 ° 48 ′ W	31.4
		80	39 ° 03 ′ N	88 ° 21 ′ W	69.7
	equal-area	θ =0	**37 ° 47 ′ N**	87 ° 22 ′ W	132.0
		10	**37 ° 48 ′ N**	87 ° 23 ′ W	129.4
		20	**37 ° 52 ′ N**	87 ° 25 ′ W	121.8
		30	**37 ° 59 ′ N**	87 ° 29 ′ W	108.4
		40	**38 ° 10 ′ N**	87 ° 33 ′ W	88.2
		50	**38 ° 25 ′ N**	87 ° 37 ′ W	60.0
		60	**38 ° 45 ′ N**	87 ° 49 ′ W	32.3
		70	39 ° 04 ′ N	88 ° 31 ′ W	84.0
		80	39 ° 07 ′ N	92 ° 29 ′ W	425.0

Table 3: Weber solutions and location errors using Japanese data

			latitude-longitude coordinate		location error
spherical solution			*35 ° 28 ′ N*	*137 ° 19 ′ E*	-
planar solution	Mercator		**35 ° 26 ′ N**	137 ° 20 ′ E	3.2
	equirectangular	θ =0	35 ° 29 ′ N	137 ° 25 ′ E	9.7
		10	35 ° 29 ′ N	137 ° 25 ′ E	9.1
		20	35 ° 28 ′ N	137 ° 24 ′ E	7.5
		30	**35 ° 27 ′ N**	137 ° 23 ′ E	5.3
		40	**35 ° 25 ′ N**	137 ° 21 ′ E	4.7
		50	**35 ° 23 ′ N**	137 ° 19 ′ E	7.7
		60	**35 ° 22 ′ N**	137 ° 19 ′ E	11.3
		70	**35 ° 20 ′ N**	137 ° 22 ′ E	14.8
		80	**35 ° 21 ′ N**	137 ° 37 ′ E	30.1
	equal-area	$\theta = 0$	35 ° 33 ′ N	137 ° 31 ′ E	20.6
		10	35 ° 32 ′ N	137 ° 31 ′ E	19.1
		20	35 ° 31 ′ N	137 ° 28 ′ E	14.9
		30	35 ° 28 ′ N	137 ° 25 ′ E	8.9
		40	**35 ° 25 ′ N**	137 ° 21 ′ E	6.3
		50	**35 ° 22 ′ N**	137 ° 20 ′ E	11.1
		60	**35 ° 20 ′ N**	137 ° 24 ′ E	16.5
		70	**35 ° 21 ′ N**	137 ° 44 ′ E	39.7
		80	**35 ° 25 ′ N**	137 ° 37 ′ E	117.6